RESEARCH ARTICLE

ADVANCED
INTELLIGENT
SYSTEMS
Open Access

www.advintellsyst.com

Miniaturized Variable Stiffness Gripper Locally Actuated by Magnetic Fields

Lukas Masjosthusmann, Michiel Richter, Pavlo Makushko, Denys Makarov, and Sarthak Misra*

In minimally invasive surgery, grippers are essential for tissue manipulation. However, in commercial tendon-driven systems, challenges remain, including tendon fatigue and bulkiness. Promising alternatives are magnetically actuated systems, offering contactless steering but limited forces. To overcome this, a miniaturized, locally actuated magnetic gripper with variable stiffness is presented. The gripper employs thin planar coils (75 μm) and a radially magnetized plunger, enabling local actuation and enhanced orientation control. The variable stiffness compliant mechanism made from shape-memory polymer facilitates different gripping strategies. In its rigid state, pulsed pulling forces of 340 mN and continuous forces of 90 mN are achieved, exceeding the gripper weight by factors of 70 and 18, respectively. The soft state, with a fast response time of 20 ms, enables soft gripping of various targets, including moving ones and rat tissue samples. Demonstrating the applicability, contactless steering and target retrieval within a stomach phantom is showcased. This study introduces promising improvements to magnetically actuated grippers for surgical procedures, addressing key challenges in current designs.

1. Introduction

Forceps and grippers play a fundamental role in manipulating tissue and exerting forces within the human body. Traditionally, forceps have been manual tools, relying on mechanical lever mechanisms. However, the rise of robotic platforms such as the DaVinci system (Intuitive Surgical Inc.),[1] Mako system (Stryker Corporation),[2] and Genesis system (Stereotaxis Inc.)[3] introduced a new era of flexibility and automation in minimally invasive surgery (MIS).

Modern grippers used for MIS utilize various actuation mechanisms, such as tendons, pneumatics, and magnetism.[4] Most commercially used are tendon-driven systems featuring rigid joint mechanisms.[5–9] Despite providing higher actuation forces compared to current alternatives, problems of tendon fatigue, system friction, and overall system bulkiness remain.[4] These challenges result in a limited lifetime capacity and hinder the development of further miniaturized systems. Widely used tendon-driven instruments, such as the EndoWrist from Intuitive Surgical, Inc., have therefore a limited capacity of up to 15 actuations. Pneumatic and hydraulic systems that use channels to avoid mechanical friction are a potential alternative for manipulating surgical tools.[10–13] However, there are limits to these systems in terms of steering and force generation.

In recent years, the utilization of magnetic fields for the manipulation of surgical instruments has gained interest. Magnetic actuation systems based on permanent magnets,[14,15] individual electromagnets,[16] or several electromagnets[17,18] were developed for this purpose. The magnetic fields employed for actuation can be generated externally or localized internally within a biological system.

Within the context of gripping, externally generated magnetic fields have found application in actuating millimeter-sized flexible grippers,[16] permanent magnet-based grippers,[19] and soft robotic grippers.[20] External magnetic fields enable contactless manipulation, whereby the performance of the instrument depends on the strength of the generated field. However, this dependency results in limited actuation forces, especially at larger working distances required for manipulating surgical instruments within a human torso.

An alternative approach is the use of local magnetic fields.[21–23] In these systems, the actuation force is generated

L. Masjosthusmann, M. Richter, S. Misra
Surgical Robotics Laboratory
Department of Biomechanical Engineering
University of Twente
7522 NB Enschede, The Netherlands
E-mail: s.misra@utwente.nl

P. Makushko, D. Makarov
Helmholtz-Zentrum Dresden-Rossendorf e.V.
Institute of Ion Beam Physics and Materials Research
Bautzner Landstraße 400, 01328 Dresden, Germany

S. Misra
Surgical Robotics Laboratory
Department of Biomaterials and Biomedical Technology
University of Groningen and University Medical Center Groningen
9713 AV Groningen, The Netherlands

The ORCID identification number(s) for the author(s) of this article can be found under https://doi.org/10.1002/aisy.202400037.

locally by permanent magnets and electromagnets. Although the use of conventional permanent magnet–coil combinations reduces power consumption, orientation control is usually limited compared to externally actuated systems. This limitation is a consequence of the axial magnetization of these systems. However, the applicable force onto a target is a remaining challenge with all magnetically actuated grippers.

To increase the functionality of grippers and other surgical instruments, the integration of smart materials, such as SMAs[24] and SMPs,[25] has gained attention. These materials exhibit the ability to revert to a predefined shape upon exposure to specific stimuli, typically temperature change. In addition, SMPs exhibit temperature-dependent stiffness, making components with controllable stiffness possible.[26,27] In order to control the temperature of these materials, heating wires or incorporated ferromagnetic[28] or conductive particles[29,30] are utilized. The adaptability of these materials enables systems with both rigid and soft properties.

In this study, we present a locally magnetically actuated miniaturized gripper based on a variable stiffness mechanism. Our developed system features several advantages. First, it does not require tendons or a high-power external actuation system. By utilizing miniature planar coils and a sliding permanent magnet, the gripper opening can be controlled independently from an external field. Unlike other systems, the magnetization of our system is perpendicular to the central axis of the employed catheter. This enables improved orientation control in comparison with conventional actuated magnetic grippers. Second, by controlling the temperature of the variable stiffness compliant mechanism (VSCM), a gripper with adaptable mechanical properties is realized. This adaptability allows targets to be envelope-gripped or pinch-gripped. In its rigid state, the gripper can exert pulsed

pulling forces of up to 340 mN and continuous pulling forces of up to 90 mN. This corresponds to around 70 and 18 times the weight of the gripper, respectively. The flexible state, on the other hand, is used to minimize possible damage when gripping soft targets. In addition, dynamic gripping of moving targets is enabled by the fast response time of 20 ms in the heated state. Finally, the compliance of the gripper structure allows for miniaturization and a higher number of actuations in comparison with tendon-driven systems. Combined with the ultrathin planar coils (75 μm), this results in a compact, locally actuated miniature gripper ($5 \times 2.5 \times 12.5$ mm³), suitable for MIS. A comparison between different actuated grippers is presented in **Table 1** to place this work in the context of the state of the art.

The performance of our gripper is evaluated by measuring the maximal applicable pulling force and the maximum opening. In addition, the adaptability of the gripper is used to manipulate a range of targets, including rat tissue samples, with different elastic properties and shapes. Finally, contactless steering and orientation control of our gripper for gripping and retrieving a soft target within a stomach phantom is shown.

2. Results

Our gripper features two main components: a hard-magnetic plunger with a planar coil-based actuation system and a temperature-responsive compliant gripping mechanism (**Figure 1**a). Both components are housed within a heat-resistant cover and affixed to a flexible catheter, making it a continuum robot.

In the following sections, a discussion is provided on the principle of local planar coil-based magnetic actuation. In addition, a characterization of the magnetic properties of our gripper is

Table 1. Comparison of grippers employing alternative actuation methods instead of tendon-driven systems.

Study[a]	Type	Volume [mm³]	Pulling force [mN mm⁻³]	Response time [s]	Soft gripping	Tip rotation
Kordmahale et al.[10]	Hydraulic	2.7	0.6	Rapid	Yes	n/a
Gao et al.[12]	Pneumatic	400	0.025	Rapid	Yes	n/a
Gerboni et al.[13]	Pneumatic	9975	0.56	Rapid	No	n/a
Wakimoto et al.[37]	Pneumatic	620	0.0035	Rapid	Yes	n/a
Kortman et al.[38]	Pneumatic	6283	0.53	Rapid	Yes	n/a
Wang et al.[39]	SMA and SMP	21 600	0.28	40/240	No	n/a
Ze et al.[28]	SMP and Magnetic	14 844	0.015	23/30	Yes	No
Nica et al.[40]	Magnetic	420	2.59	0.7	No	No
Lim et al.[41]	Magnetic	80	60 mT: 0.45	Rapid	No	Yes
Shao et al.[21]	Magnetic (local)	3341	3×10^{-7}	Rapid	Yes	No
Ulrich et al.[22]	Magnetic (local)	1250	0.04	Rapid	No	No
Do et al.[23]	Magnetic (local)	478	0.0003	Rapid	Yes	No
Our gripper	SMP and Magnetic (local)	156	P: 2.17 S: 0.58	10/23	Yes	Yes

[a]The methods investigated include hydraulic, pneumatic, shape-memory alloy (SMA), shape-memory polymer (SMP), and magnetic-based systems. The volume corresponds to the package size of the respective system. The pulling force corresponds to the maximum force that can be applied to a target. In cases where only the closing force of the gripper is specified, it is assumed that this force can be fully converted into equivalent maximum pulling forces. This assumption is based on the results of a study by Li et al. in which the friction coefficient between a minimally invasive gripper and liver tissue was measured.[42] For our gripper, we differentiate between pulsed pulling (P) and steady pulling (S), while n/a implies "not applicable." Two response times are specified for thermally actuated grippers (heating time/cooling time).
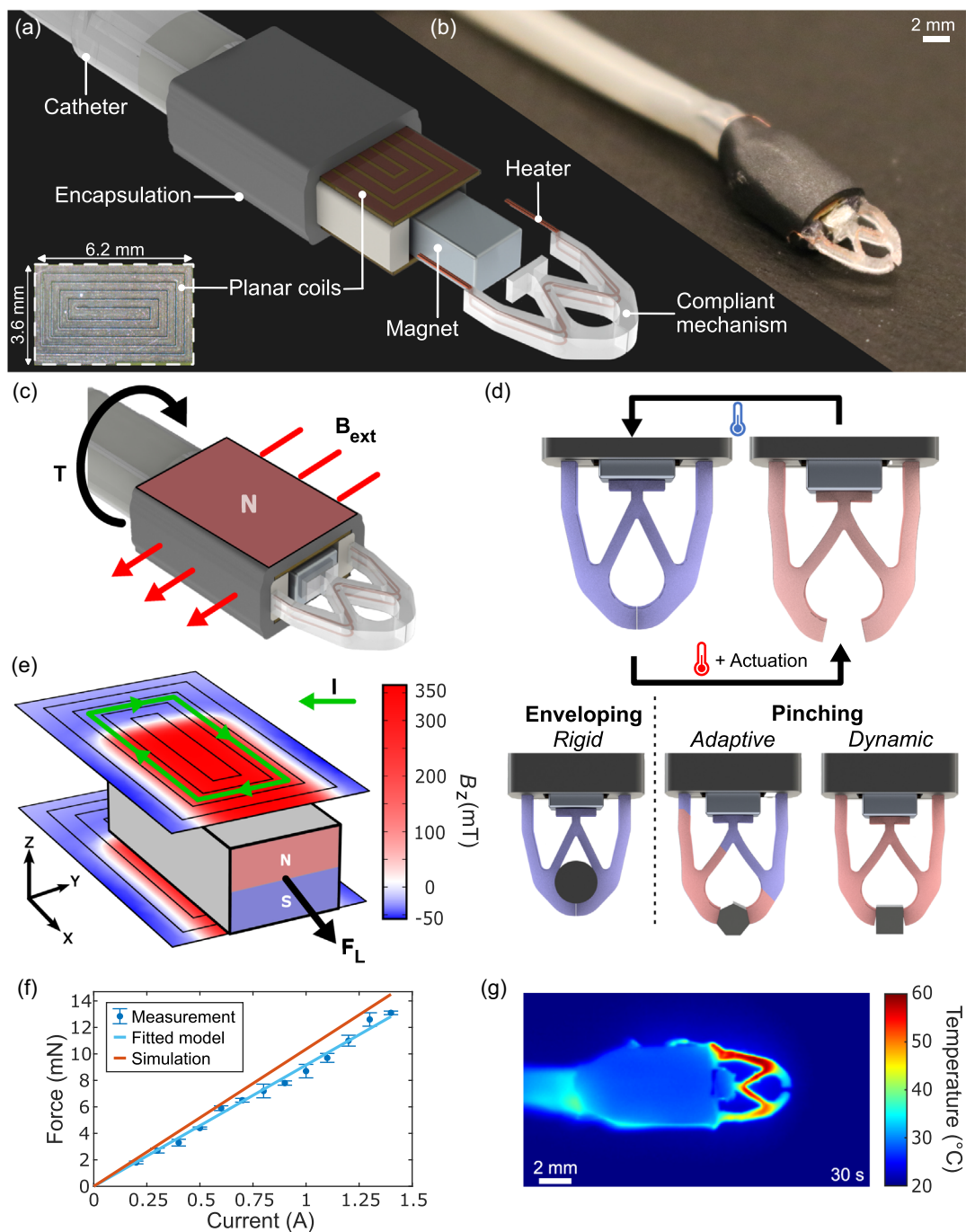
Figure 1. Mechanisms of the locally actuated variable stiffness gripper. a) Illustration of the gripper including all core components. b) Fabricated and assembled prototype of the gripper c) Display of magnetization of the proposed design and applicable torque (**T**) along the axis of the catheter when applying an external field (**B**$_{ext}$). d) Illustration of the heat-dependent states of the proposed compliant structure. By heating the structure and applying an actuation force, the structure is deformed. e) Simulation of the magnetic field (B$_z$) in z-direction. Schematic display of the actuation principle based on the Lorentz force (**F**$_L$) resulting from the interaction of the magnetic field and the coil current (I). f) Current-depending force estimated by the electromagnetic model and measured with a force sensor. g) Thermal image of the compliant structure after 30 s of heating while a continuous 0.35 A current is applied to the inserted thin copper wire (⌀20 μm).

provided, including the field of the hard-magnetic plunger and the thereby exerted Lorentz force on the planar coils. Thereafter, the design and temperature-dependent stiffness properties of the

SMP-based gripping mechanism are presented. Then, two different gripping modes are shown: enveloping and pinching, which are subsequently used to demonstrate gripping targets with

**ADVANCED
SCIENCE NEWS**

www.advancedsciencenews.com

**ADVANCED
INTELLIGENT
SYSTEMS**
Open Access

www.advintellsyst.com

different shapes and stiffness, including rat tissue samples (Figure 1d). Finally, the additional functionality of the hard-magnetic plunger as a point of actuation for external magnetic fields is shown by steering the gripper through a mock-up of the human stomach.

2.1. Local Magnetic Actuation

The first main component consists of a radially magnetized hard-magnetic plunger, surrounded by a pair of two-sided square planar coils (Section S1, Supporting Information). The proposed actuation system relies on the local interaction between the magnetic field ($\mathbf{B} = [B_x, B_y, B_z]^T$, $B_{xyz} \in \mathbb{R}$) generated by the hard-magnetic plunger and the current density ($\mathbf{J} \in \mathbb{R}^3$) through planar coils, which generates a Lorentz force ($\mathbf{F}_L = \mathbf{J} \times \mathbf{B}$). The planar coils, which are fixed in their position, generate a force acting on the plunger and thus induce its motion (Figure 1e). This motion ultimately leads to the deformation of the compliant gripping mechanism.

The configuration of planar coils and plunger is such to maximize the Lorentz force. To this end, a local reference frame ($\mathbf{R} = [\hat{\mathbf{x}}, \hat{\mathbf{y}}, \hat{\mathbf{z}}] \in \mathbb{R}^3$) is defined between the planar coils (Figure 1e). The two double-sided coils are located at $\mathbf{p}_{c1} = 0.5h\hat{\mathbf{z}}$ and $\mathbf{p}_{c2} = -0.5h\hat{\mathbf{z}}$, and the magnetic plunger at $\mathbf{p}_m = a\hat{\mathbf{x}}$, where $h, a \in \mathbb{R}$ represent the constant plunger height and variable displacement relative to the coil center, respectively. Then, within the reference frame ($\mathbf{R}$) the planar coils are stationary, such that at constant coil current the Lorentz force ($\mathbf{F}_L$) is only depending on the field ($\mathbf{B}$) of the displaced plunger.

A parametric sweep ($a \in [0, 4]$ mm) of the reference plunger displacement is performed numerically (MATLAB R2023) to maximize $\mathbf{F}_L$. At equal constant coil currents $I = 1$ A, an optimal offset of $a = 1.3$ mm is found (Figure S1, Supporting Information). The corresponding simulated $\mathbf{F}_L$ acting on the magnetic plunger at the reference displacement is simulated to be 11.2 mN.

The electromagnetic model (Section S2, Supporting Information) is validated using a prototype, whereby the Lorentz force is measured at different currents ($I \in [0, 1.4]$ A). While for an equal constant offset of $a = 1.3$ mm the model predicts a force of 10.4 mN A^{-1}, measurements show a slightly lower force of 9.2 mN A^{-1} (Figure 1f). This discrepancy is mainly due to occurring friction within the actuation system. Finally, the model predicts a peak force of 14.5 mN at $I = 1.4$ A ($P = 3.9$ W), which is close to the experimental result of 13.1 mN. This peak Lorentz force serves as a key parameter influencing the design of the VSCM.

2.2. VSCM

The second main component of our system is the compliant gripper made from SMP (**Figure 2**a). The VSCM fulfills two essential requirements. First, it offers flexibility to deform in response to the Lorentz force ($\mathbf{F}_L$). Second, it provides rigidity to exert a higher pulling force than in the soft state on an enveloped target (Figure 1d). This variable stiffness is attained by exploiting the material properties of NOA63, a biocompatible, UV-curable polyurethane-based SMP.

The design of the VSCM is based on a topology optimization that maximizes the opening of the gripper against $\mathbf{F}_L$ (Figure 2b and Section S3, Supporting Information). The resulting shape resembles a normally closed two-finger gripper (Figure S5,
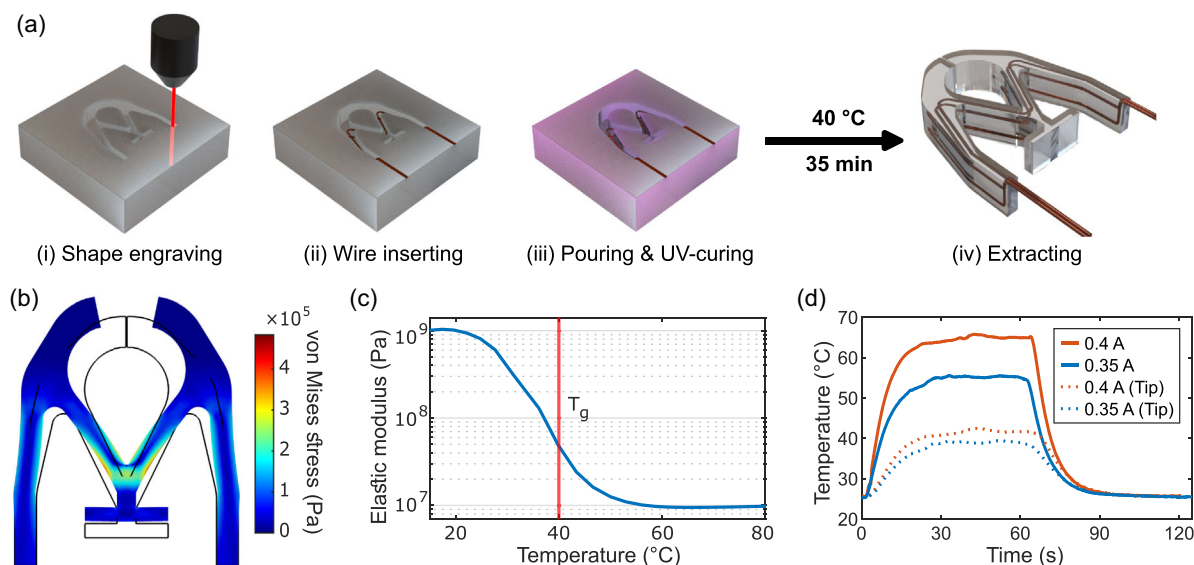
Figure 2. Realization of compliant variable stiffness mechanism. a) Fabrication of the SMP-based compliant structure: i) laser-engraving of the targeted shape into PDMS sheet. The PDMS sheet is prepared in advance also by molding. ii) Manual insertion of the thin copper wire (Ø20μm) for local temperature control of the structure. iii) Pouring of the SMP and UV-curing at 40 °C. iv) Extraction of the molded structure. b) Simulation of the mechanical stresses and displacements occurring in the compliant structure employed, induced by an acting Lorentz force of 13.1 mN. c) Temperature-dependent elastic modulus of the employed SMP with a transition temperature (T_g) of 40 °C. d) Measured heating and cooling cycles of the compliant structure for applied currents of 0.35 and 0.4 A. The straight lines correspond to the maximum measured temperature, while the dotted lines correspond to the temperature at the fingertips.

Supporting Information). The overall VSCM measures 4 mm in width, 4.5 mm in length, and 0.9 mm in thickness, with a minimum feature width of 0.3 mm. Further, the VSCM is fabricated with a biocompatible UV-curable polyurethane-based SMP.[31] To control the stiffness of the VSCM, local Joule heating is realized with an integrated copper wire (⌀20 μm, Figure 1g). The use of a thin inserted copper wire provides two advantages over incorporating ferromagnetic or conductive particles. First, the impact of the wire on the mechanical properties of SMP is negligible compared to those with added particles described in the literature. Second, the simplicity of the heating mechanism as there is no need for an additional induction coil or extra insulation layers.

The elastic modulus (E) of the employed SMP depends on the temperature. In this study, the transition temperature (T_g) of the SMP is set to 40 °C by controlling the ambient temperature during the curing process.[32] The elastic modulus is experimentally characterized for a range of temperatures ($T \in [18, 80]$ °C) (Figure 2c and Section S4, Supporting Information). At room temperature ($T_{cold} \leq 20$ °C), the VSCM is in the glass state ($E_{cold} \approx 1$ GPa). Upon heating, the material undergoes a phase transition. Once the VSCM changes to the rubbery state ($T_{hot} \geq 54$ °C), the elastic modulus decreases significantly ($E_{hot} \approx 10$ MPa).

To estimate the required heating current and transition time, the time-dependent temperature variation of the VSCM at room temperature is measured for different applied currents (Figure 2d). At room temperature, Joule heating toward a temperature transition $T_{cold} \rightarrow T_{hot}$ requires 10 s at a current of 0.4 A. Passive cooling for $T_{hot} \rightarrow T_{cold}$ requires 23 s. Although our gripper has a faster response time than other thermally actuated grippers, the initial response time is slower than systems that do not require heating.

In the heated state, the elastic modulus is in the range or even softer than various human tissues such as cartilage ($E = 1$ MPa), skin ($E = 26$ MPa), and muscle ($E = 350$ MPa).[33] Therefore, the risk of damage when interacting with these tissues is mitigated. Furthermore, due to the local character of the integrated heating mechanism, the temperature at the fingertips remains significantly lower ($T_{tip} = 38$ °C, Figure 1g and 2d). This has the advantage of minimizing heat transfer to the target, reducing potential thermal damage to surrounding tissue.

2.3. Variable Stiffness Gripping

The combination of the local magnetic actuation system with the VSCM results in a controllable gripper. Based on the state of the local actuation system and the stiffness of the compliant mechanism, different gripping strategies can be realized. In the following sections, we will introduce our approach to envelope gripping and pinch gripping.
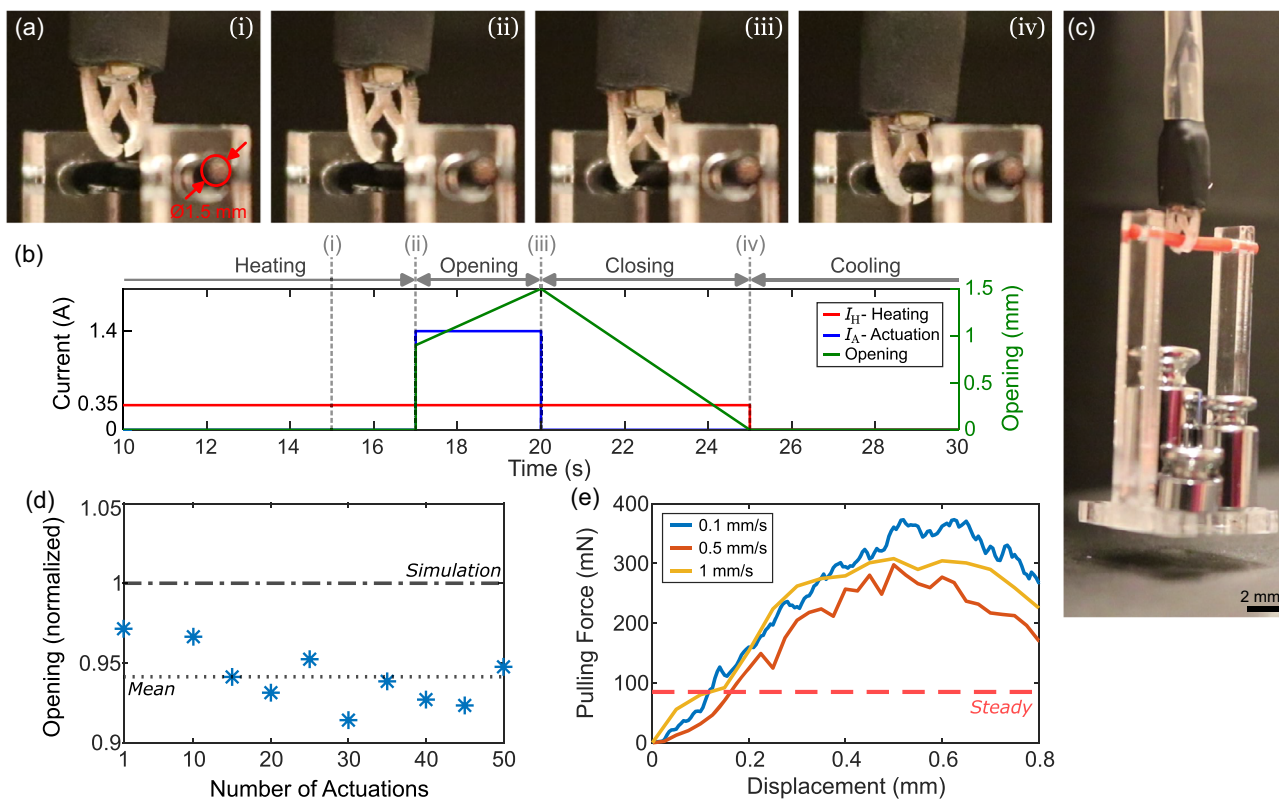

Figure 3. Characterization of envelope gripping capabilities. a) Enveloping a cylindrical target (⌀1.5 mm) larger than the maximum aperture by utilizing the shape and softness of the fingertips: i) closed state, ii) fully opened, iii) additional deformation, and iv) closed state. b) Controlled heating (I_H) and actuation (I_A). c) Pull and hold a load of 9 g. d) Comparison of opening after multiple actuations ($N = 50$) with the simulated opening. The opening is normalized to the simulated opening (0.9 mm). e) Measurement of the pulling force when displacing the gripper with a certain speed. The steady pulling force corresponds to the force that can be lifted continuously. All measurements are done at a temperature of 20 °C.

**ADVANCED
SCIENCE NEWS**

www.advancedsciencenews.com

**ADVANCED
INTELLIGENT
SYSTEMS**

Open Access

www.advintellsyst.com

2.3.1. Envelope Gripping

The first gripping strategy investigated is the enveloping of targets. For this, both the soft and rigid states of the gripper are used. In the context of envelope gripping, two aspects are investigated: the maximum opening and the maximum applicable pulling force.

The first aspect is the maximum opening of the gripper, which determines the size range of possible targets that can be gripped. At an actuating current of 1.4 A, a maximum opening of 0.875 mm is measured (**Figure 3**a). However, due to the flexibility and shape of the fingertips, the gripper can envelop objects that are twice as large as this maximum opening (Figure 3b and Movie S1, Supporting Information). In addition, the repeatability of this opening motion is investigated (Figure 3d). After

actuating the gripper 50 times, the opening is reduced by only 2.5%, which underlines the repeatability of the gripping mechanism, especially when compared to the limited lifetime of tendon-driven instruments.

The second investigated aspect is the maximum pulling force that can be applied. For this, we measure the force applied as the gripper is continuously pulled until a deformation occurs, leading to a subsequent opening. Additionally, we determine the maximum load that the gripper could sustain continuously. Experimental results demonstrate that peak pulling forces of up to 340 mN (2.17 mN mm^{-3}, Figure 3e) can be exerted at room temperature while consistently lifting a load of 9 g (0.58 mN mm^{-3}, Figure 3c). This load corresponds to 70 times and 18 times the weight of the gripper, respectively, exceeding the current force-to-volume ratios of locally magnetically actuated
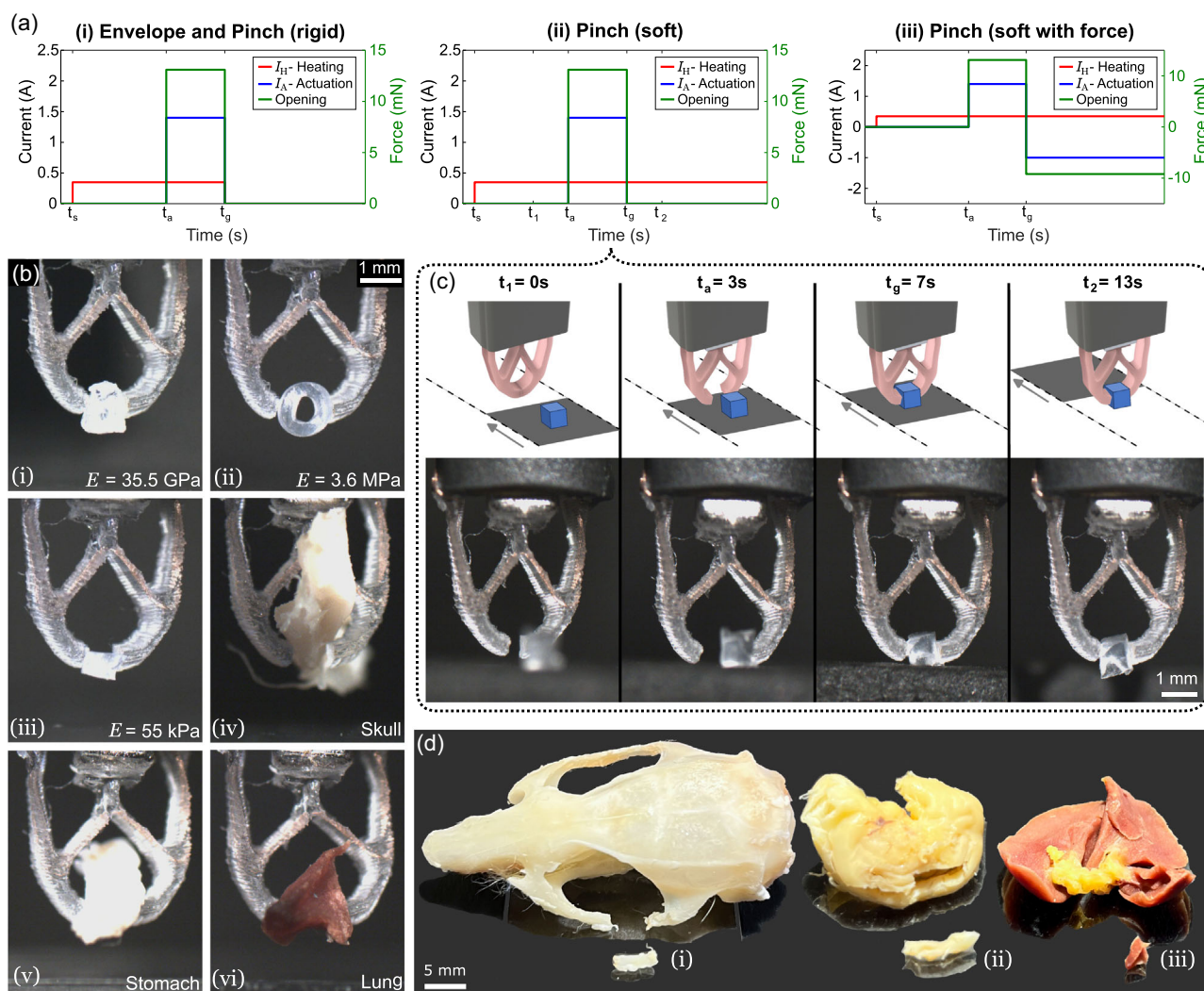

Figure 4. Adaptive gripping of various targets. a) Strategies for different gripping modes based on the applied heating current (I_H) and the actuating current (I_A) resulting in varying Lorentz forces. b) Pinch gripping of different objects with varying elastic moduli (E) and shapes: i) NaCl crystal $E = 35.5$ GPa,[36] ii) silicone tube $E = 3.6$ MPa, iii) Ecoflex 00-20 cube $E = 55$ kPa (Smooth-On Inc., United States), and iv–vi) gripping and lifting of rat tissue and bone samples. c) Demonstration of dynamic gripping of a moving Ecoflex 00-20 cube. The gripper is initially heated and thus in a soft state. The target and floor move at a steady 3 mm s^{-1} into the image. As the target approaches the gripper, the local actuation system is used to open the compliant structure. When the target is in between the fingertips, deactivation of the actuation system causes a closing. d) Display of fixated rat tissue and bone samples: i) skull, ii) stomach, and iii) lung.

grippers. In comparison, Bekeny et al. conducted force measurements on a surgical tool during the in vitro resection of a tumor from a skull.[34] Their study showed average interaction forces of 100–150 mN between the surgical tool and the in vitro environment. These results show the potential of our gripper in terms of interaction force for application in MIS.

2.3.2. Pinch Gripping

Our gripper can not only be used for enveloping but also allows pinch gripping of various targets. Different pinch-gripping strategies are realized by adjusting the state of actuation and heating after closing the gripper (**Figure 4**a). All gripping strategies require an initial heating phase to soften the gripper and allow for deformation. This softness of the gripper is then used to adapt the fingertips to the shape and the mechanical properties of the target object. After pinching a target, the gripper can be cooled or maintained in the heated state to enable the dynamic release. Moreover, the softened state allows for an increased pinch force through an additional closing force generated by the local actuation system. This resulting adaptability of our gripper is demonstrated through gripping tests on targets with different mechanical properties.

First, the performance of the gripper when interacting with objects exhibiting different elasticity moduli is tested. It is shown that the gripper can interact and lift a range of materials,

including rigid targets (NaCl crystal, $E = 35.5$ GPa), soft targets (silicone tube, $E = 3.6$ MPa), and very soft targets (Ecoflex cube, $E = 55$ KPa) (Figure 4b and Movie S2, Supporting Information). The elastic moduli of these targets cover a wide range of elastic moduli found in biological tissue, from cartilage to bone.[33]

Second, the capability to manipulate targets with surgery-specific shapes is investigated (Figure 4d). We demonstrate that rat tissue and bone samples with varying shapes and sizes can be gripped and transported, including fixated lung and stomach tissue. These demonstrations highlight the adaptability of the gripper in the handling of objects of different sizes, shapes, and mechanical properties.

Finally, we investigate the capability to interact with moving targets (Movie S3, Supporting Information). For this, the gripper is continuously heated. Thus, once the gripper is heated, the system dynamics depend primarily on the dynamics of the local actuation system. Utilizing the fast response of 20 ms (Figure S6, Supporting Information) of our system, we can grip a moving target at a speed of 3 mm s^{-1} (Figure 4d). The capability to dynamically interact with targets significantly increases the functional versatility of our system compared to other SMP-based systems.

2.4. Magnetic Steering

To enable application in MIS, the gripper must reach deep targets within the human body. For this, we extend the system
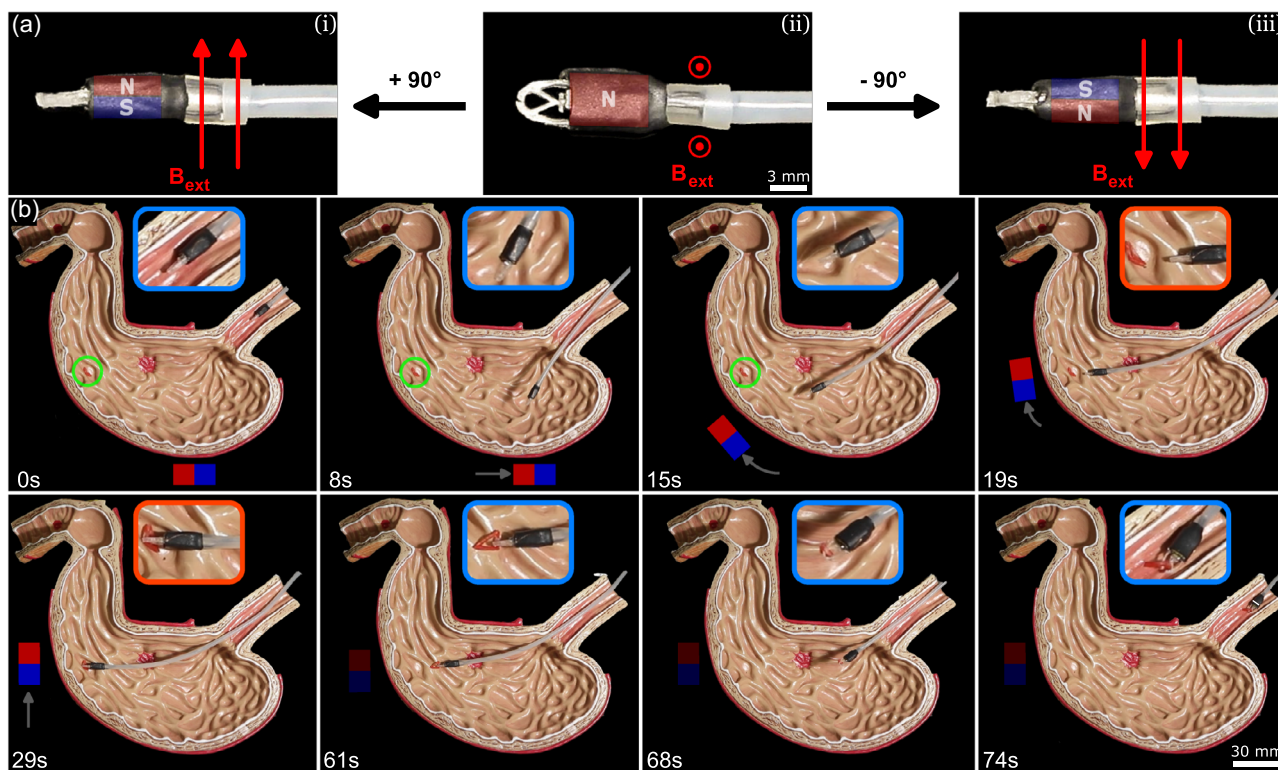

Figure 5. Contactless steering and target retrieval. a) Manipulation of the orientation of the fingertips by changing the direction of the external magnetic field (B_{ext}). A handheld permanent magnet is used to generate the external field. The red arrows indicate the direction of the applied magnetic field. b) Demonstration of magnetic steering and controlled gripping within a stomach phantom. The gripper is manually guided toward the red triangle-shaped silicone target using an external magnetic field. Once the target is reached, the gripper is heated for 15 s, opened, and pushed forward to envelop it. After enveloping, the gripper is cooled down for 20 s, followed by the retrieval of the target by pulling the gripper.

**ADVANCED
SCIENCE NEWS**

www.advancedsciencenews.com

**ADVANCED
INTELLIGENT
SYSTEMS**
Open Access

www.advintellsyst.com

with a 2.5 mm diameter flexible silicone catheter. The employed catheter, with the hard-magnetic plunger as a point of actuation, can be contactlessly steered using an externally applied field. The flexibility of the catheter used minimizes disturbances of potential environmental movements and improves the maneuverability of the system in complex environments.[35]

The external field ($\mathbf{B}_{ext}$) generated by a manually operated permanent magnet induces a torque ($\mathbf{T} = \mathbf{m} \times \mathbf{B}_{ext}$), acting on the gripper. Using the local reference frame ($\mathbf{R}$), the magnetic plunger is magnetized perpendicular to the affixed catheter ($\mathbf{m} = [0, 0, m_z]^T$, $m_z \in \mathbb{R}$). This direction of magnetization allows torques to be applied in the x- and y-directions. The torque in the x-direction can be used to align the gripper with the target, a motion that is not possible with conventional magnetized systems ($\mathbf{m}_c = [m_x, 0, 0]^T$, $m_x \in \mathbb{R}$). This ability to rotate the gripper around the x-axis is demonstrated in **Figure 5**a. The orientation of the fingertips can be controlled within 180 degrees, realizing every potential gripping scenario.

Finally, we demonstrate the capability to contactlessly steer the gripper through a 3D stomach phantom (Figure 5b and Movie S4, Supporting Information). The gripper with the affixed catheter is steered toward the target. After reaching it, the compliant mechanism is heated and the coils are activated. By advancing the catheter, the target is enveloped, allowing subsequent gripper closure and cooling. The target is then retrieved from the stomach phantom. In summary, we have qualitatively demonstrated the functionality of both the steering and gripping processes in a 3D environment.

3. Conclusions

We report the design and evaluation of a miniaturized, locally actuated magnetic gripper employing a compliant mechanism based on SMP. The system features ultrathin planar coils (75 μm) and a hard-magnetic plunger, resulting in a space-efficient local actuation mechanism with magnetization oriented perpendicular to the affixed catheter. The presented design enables improved contactless orientation control of the fingertips, exceeding the capabilities of conventional local magnetic actuation systems. By integrating a VSCM with the local actuation system, we realize a gripper with adaptive mechanical properties, which allows the implementation of different gripping strategies depending on the respective target.

The developed miniaturized gripper exhibits the capability to grip diverse targets while in its rigid or soft state. In the rigid state, the gripper can exert pulling forces of up to 340 mN, exceeding the current capabilities of locally actuated grippers in terms of size and force per volume (2.17 mN mm^{-3}). Moreover, the gripper can be operated continuously in the soft state. The system response in this state is as fast as 20 ms, enabling pinch gripping of moving targets. Operating independently of large external systems, the gripper can easily be integrated into surgical procedures, requiring only 5 W for full functionality. Furthermore, commercially available magnetic-based surgical systems can directly be used to provide the necessary magnetic field for contactless steering of the gripper. We validate the performance of the gripper through quantitative and qualitative experiments, showcasing its ability to grip and lift

rat tissue samples. Additionally, we demonstrate its applicability by achieving contactless steering in a stomach phantom to retrieve a target.

The force-to-volume ratio can be further increased by using a customized plunger and more advanced assembly strategies. This opens up the potential for application in different environments, such as use in the brain or cardiovascular system. Moreover, the rectangular cross section provides space for additional components without increasing the maximum external dimensions. The integration of a miniature camera, light sources, or sensors to measure interaction forces mitigates potential harm and eliminates the need for large tracking systems. We are convinced that the use of surgical grippers and instruments in general based on variable stiffness mechanisms and local magnetic actuation can improve the ability to adapt and therefore simplify complex surgical procedures.

4. Experimental Section

Fabrication of Planar Coils: The local actuation system design employed a pair of two-sided coils. In the first step, single-side planar coils were made from polyimide copper laminate (DuPont Kapton, IM30-LM-000122, Goodfellow GmbH, Germany) with a polymer thickness of 25 μm and a copper thickness of 18 μm. In this study, rectangular-shaped coils were used, measuring 6.2 mm in length and 3.6 mm in width with a resistance of ≈0.4 Ω. The layout of the electromagnetic coils was realized by wet etching and image-reversal optical lithography. For this, the copper surface was cleaned for 2 min using O_2 oxygen plasma. Image reversal photoresist (AZ5214e, MicroChemicals GmbH, Germany) was first spin-coated at 1000 rpm for 30 s and then baked for 2 min at 110 °C. Subsequentially, the spin-coated layer was patterned by a UV laser writer (DWL66, Heidelberg Instruments, Germany) with a wavelength of 410 nm. It was then flood-exposed to UV light and developed in the AZ351b developer. Finally, the coils were postbaked for 5 min at 120 °C and wet etched in 1:10 sodium persulfate solution in deionized (DI) water (B327, AG TermoPasty, Grzegorz Gasowski, Poland) kept at 60 °C. Any remaining etching agent was removed with DI water and the photoresist with acetone, isopropanol, and DI water. The rear sides of two single-sided coils were then bonded together using adhesive (Loctite 401, Henkel Corp., Germany). Once the adhesive was solidified, the coil stack was thinly coated with high-temperature resin (RS-F2-HTAM-02, Formlabs, United States) and cured using UV-C light for 30 min at 40 °C. Finally, the front and rear sides were interconnected, and both two-sided coils were connected in series.

Fabrication of Variable Stiffness Mechanism: The miniaturized VSCM was produced by molding the desired shape with a biocompatible, UV-curable polyurethane-based SMP (NOA63, Norland Products Inc., United States).[31] Initially, a self-curing SMP (MP3510, SMP Technologies Inc., Japan) was used. However, the short curing time of this material limited the molding of small structures without trapping air bubbles. Therefore, NOA63 was used, a material that only cured when exposed to UV-A light. This simplified the manufacturing process, as the SMP poured into the molds can be degassed over a longer period of time without curing. In addition, the variable transition temperature of NOA63 increased the design flexibility by allowing not only the shape but also the mechanical properties of the compliant structures to be adapted. The molds for the compliant structure were made from 2 mm-thick polydimethylsiloxane (PDMS) (Sylgard 184, Dow, United States) sheets, which themselves underwent a molding procedure. These sheets were made by mixing PDMS at a 10:1 volume ratio of base-curing agent. After curing, the shape of the compliant structure was laser engraved (Speedy 300, Trotec Laser, Austria) into the prepared PDMS sheets. To avoid excessive heating, three successive engraving steps were performed to achieve the desired engraving depth. After engraving, the molds were thoroughly cleaned with DI

water to eliminate debris, maintaining the shape of the mold and preventing SMP contamination. Subsequently, a 20 µm thin copper wire was affixed to the mold base and inserted into the engraved mold cavity. Then, the SMP was poured into this cavity, ensuring complete filling of the mold. Vacuuming the mold for 5 min at 100 mbar removed any air bubbles, resulting in a uniform SMP distribution. Excess material was carefully removed, and additional SMP was added if necessary. For curing, the mold with the poured SMP was preheated for 5 min at 40 °C, followed by a 30 min UV-A light exposure at 40 °C. Afterward, the SMP was solidified and fully cured. Upon cooling, the compliant structure was extracted from the PDMS mold. Finally, the gripper fingertips were manually separated by a thin cut.

Validation of Electromagnetic Model: The Lorentz force generated by the local magnetic actuation system was measured using a custom-built setup. The setup included a force sensor (K3D40a, ME-Messsysteme GmbH, Germany), a signal amplifier (GSV-4USB, ME-Messsysteme GmbH, Germany), and a support structure for positioning the magnet and actuator. The support structure was made of laser-cut polymethyl methacrylate components assembled with glue and screws. The magnet was placed on the support structure and subjected to a downward force from interaction with planar coils. Before force measurement, the weight of the magnet and support structure was compensated for. To ensure statistical reliability, each measurement was repeated 8 times per current step. All measurement data were filtered using a finite impulse response filter.

Measurement of Pulling Force: The pulling force was measured using the same sensor and signal amplifier employed for the validation of the electromagnetic model. The previous support structure was replaced by a structure with an integrated rod with a diameter of 0.9 mm (Figure S8, Supporting Information). The rod functioned as the target to be enveloped and pulled. For force measurement, the compliant structure, plunger, and adapted housing were connected to a mobile robotic arm (UR5e, Universal Robots, Denmark). The force sensor, affixed to the target, remained stationary during all tests. To determine the maximum pulling force, the robotic arm, equipped with the gripper, was moved vertically with a constant velocity. Pulling at three different velocities was tested (0.1, 0.5, and 1 mm s^{-1}). Each pulling test purposely resulted in forceful deformation and subsequent release of the enveloped target. The occurring force was continuously measured while moving the arm upward. For statistical reliability, each measurement was repeated 5 times per velocity step. All measurement data were filtered using a finite impulse response filter.

Demonstration of Magnetic Steering: The demonstration was performed in an anatomical model of the stomach (193 × 30 × 156 mm^3), and 3D printed elastic triangle of size 4 mm was used as a target. The gripper was manually steered toward the target with a permanent magnet. For this, a bar-shaped neodymium permanent magnet (Q-111-89-20-E, Webcraft GmbH, Germany) was used, and the applied magnetic field was around 40 mT. The forward and backward motion of the gripper was realized by manually pushing and pulling the end of the catheter.

Temperature Measurements: All thermal measurements and images were made using an infrared camera (Ti400, Fluke Corporation, United States). The measurement data were then analyzed and displayed using MATLAB R2023.

Control and Power System: To control the actuation and heating currents, a programmable DC power supply (E36313A, Keysight Technologies, United States) was used for all experiments. The operating current was controlled by limiting the current.

Supporting Information

Supporting Information is available from the Wiley Online Library or from the author.

Acknowledgements

Conflict of Interest

The authors declare no conflict of interest.

Data Availability Statement

The data that support the findings of this study are available from the corresponding author upon reasonable request.

Keywords

[1] G. Guthart, J. Salisbury, in *Proc. 2000 IEEE Int. Conf. on Robotics and Automation*, San Francisco **2000**.

[2] C. Batailler, A. Fernandez, J. Swan, E. Servien, F. S. Haddad, F. Catani, S. Lustig, *Knee Surg. Sports Traumatol. Arthroscopy* **2021**, *29*, 3585.

[3] J. Hwang, J. Y. Kim, H. Choi, *Intell. Serv. Rob.* **2020**, *13*, 1.

[4] H. M. Le, T. N. Do, S. J. Phee, *Sens. Actuators A: Phys.* **2016**, *247*, 323.

[5] Y. Sun, Y. Liu, L. Xu, Y. Zou, A. Faragasso, T. C. Lueth, *IEEE Rob. Autom. Lett.* **2020**, *5*, 1095.

[6] D. Zhang, Y. Sun, T. C. Lueth, *Int. J. Comput. Assisted Radiol. Surg.* **2021**, *16*, 1615.

[7] T. Kato, I. Okumura, H. Kose, K. Takagi, N. Hata, *Int. J. Comput. Assisted Radiol. Surg.* **2016**, *11*, 589.

[8] C. Culmone, K. Lussenburg, J. Alkemade, G. Smit, A. Sakes, P. Breedveld, *Materials* **2021**, *14*, 7910.

[9] C. Li, Y. Yan, X. Xiao, X. Gu, H. Gao, X. Duan, X. Zuo, Y. Li, H. Ren, *IEEE Rob. Autom. Lett.* **2021**, *6*, 5541.

[10] B. S. Kordmahale, J. Qu, A. Muliana, J. Kameoka, *Sci. Rep.* **2022**, *12*, 21403.

[11] R. Lathrop, M. Ourak, J. Deprest, E. V. Poorten, *J. Med. Rob. Res.* **2022**, *7*, 2241007.

[12] H. Gao, Y. Zou, S. Huang, W. Chen, A. Gao, in *Proc. 2022 IEEE Int. Conf. on Robotics and Biomimetics*, Xishuangbanna **2022**.

[13] G. Gerboni, M. Brancadoro, G. Tortora, A. Diodato, M. Cianchetti, A. Menciassi, *Smart Mater. Struct.* **2016**, *25*, 105025.

[14] G. Ciuti, P. Valdastri, A. Menciassi, P. Dario, *Robotica* **2010**, *28*, 199.

[15] G. Mao, M. Drack, M. Karami-Mosammam, D. Wirthl, T. Stockinger, R. Schwödiauer, M. Kaltenbrunner, *Sci. Adv.* **2020**, *6*, eabc0251.

[16] F. Ongaro, C. Yoon, F. Van den Brink, M. Abayazid, S. H. Oh, D. H. Gracias, S. Misra, in *Proc. 2016 IEEE Int. Conf. on Biomedical Robotics and Biomechatronics*, Singapore **2016**.

[17] J. Sikorski, C. M. Heunis, F. Franco, S. Misra, *IEEE Trans. Magn.* **2019**, *55*, 1000305.

[18] M. P. Kummer, J. J. Abbott, B. E. Kratochvil, R. Borer, A. Sengul, B. J. Nelson, *IEEE Trans. Rob.* **2010**, *26*, 1006.

[19] C. Forbrigger, A. Lim, O. Onaizah, S. Salmanipour, T. Looi, J. Drake, E. D. Diller, *IEEE Rob. Autom. Lett.* **2019**, *4*, 1202.

[20] P. Lloyd, T. L. Thomas, V. Kalpathy Venkiteswaran, G. Pittiglio, J. H. Chandler, P. Valdastri, S. Misra, *IEEE Rob. Autom. Lett.* **2023**, *8*, 3262.

[21] G. Shao, H. O. T. Ware, J. Huang, R. Hai, L. Li, C. Sun, *Addit. Manuf.* **2021**, *38*, 101834.

[22] F. Ullrich, K. S. Dheman, S. Schuerle, B. J. Nelson, in *Proc. 2015 IEEE Int. Conf. on Robotics and Automation*, Seattle **2015**.

[23] T. N. Do, H. Phan, T. Q. Nguyen, Y. Visell, *Adv. Funct. Mater.* **2018**, *28*, 1800244.

[24] D. Braun, D. Weik, S. Elsner, S. Hunger, M. Werner, W. G. Drossel, *Materials* **2021**, *14*, 5111.

[25] C. Linghu, S. Zhang, C. Wang, K. Yu, C. Li, Y. Zeng, H. Zhu, X. Jin, Z. You, J. Song, *Sci. Adv.* **2020**, *6*, eaay5120.

[26] T. L. Thomas, J. Bos, J. J. Huaroto, V. Kalpathy Venkiteswaran, S. Misra, *Adv. Intell. Syst.* **2024**, *6*, 2200465.

[27] M. Mattmann, Q. Boehler, X. Z. Chen, S. Pane, B. J. Nelson, in *Proc. 2022 IEEE Int. Conf. on Intelligent Robots and Systems*, Kyoto **2022**.

[28] Q. Ze, X. Kuang, S. Wu, J. Wong, S. M. Montgomery, R. Zhang, J. M. Kovitz, F. Yang, H. J. Qi, R. Zhao, *Adv. Mater.* **2020**, *32*, 1906657.

[29] M. Lalegani, M. Bodaghi, *Sens. Actuators A Phys.* **2023**, *349*, 114063.

[30] M. Lalegani, M. Bodaghi, *Int. J. Adv. Manuf. Technol.* **2023**, *126*, 35.

[31] K. A. Davis, K. A. Burke, P. T. Mather, J. H. Henderson, *Biomaterials* **2011**, *32*, 2285.

[32] A. M. Diorio, X. Luo, K. M. Lee, P. T. Mather, *Soft Matter* **2011**, *7*, 68.

[33] D. Rus, M. T. Tolley, *Nature* **2015**, *521*, 467.

[34] J. R. Bekeny, P. J. Swaney, R. J. Webster, P. T. Russell, K. D. Weaver, *J. Neurol. Surg. Part B: Skull Base* **2013**, *74*, 337.

[35] M. Russo, S. M. H. Sadati, X. Dong, A. Mohammad, I. D. Walker, C. Bergeles, K. Xu, D. A. Axinte, *Adv. Intell. Syst.* **2023**, *5*, 2200367.

[36] R. A. Bartels, D. E. Schuele, *J. Phys. Chem. Solids* **1965**, *26*, 537.

[37] S. Wakimoto, K. Suzumori, K. Ogura, *Adv. Rob.* **2011**, *25*, 1311.

[38] V. G. Kortman, A. Sakes, G. Endo, P. Breedveld, *Bioinspiration Biomimetics* **2023**, *18*, 046004.

[39] W. Wang, S. H. Ahn, *Soft Rob.* **2017**, *4*, 379.

[40] M. Nica, C. Forbrigger, E. Diller, *IEEE Trans. Mechatron.* **2022**, *27*, 5541.

[41] A. Lim, A. Schonewille, C. Forbrigger, T. Looi, J. Drake, E. Diller, *IEEE Trans. Biomed. Eng.* **2021**, *68*, 846.

[42] W. Li, Z. G. Jia, J. Wang, L. Shi, Z. R. Zhou, *Tribol. Int.* **2015**, *81*, 190.